Wiley Online Library
Early View publication on www.wileyonlinelibrary.com
(issue and page numbers not yet assigned;
citable using Digital Object Identifier – DOI)

J. Biophotonics 1–8 (2016) / **DOI** 10.1002/jbio.201500315

Journal of BIOPHOTONICS

FULL ARTICLE

SPR-based plastic optical fibre biosensor for the detection of C-reactive protein in serum

*Ayda Aray***, [1], *Francesco Chiavaioli***, [2], *Mojtaba Arjmand*[1], *Cosimo Trono**, [2], *Sara Tombelli*[2], *Ambra Giannetti*[2], *Nunzio Cennamo*[3], *Mahmood Soltanolkotabi*[1], *Luigi Zeni*[3], *and Francesco Baldini*[2]

[1] Quantum Optics Group, Department of Physics, University of Isfahan, Hezar Jarib street, 98311 Isfahan, Islamic Republic of Iran
[2] Institute of Applied Physics "Nello Carrara", National Research Council, Via Madonna del Piano 10, 50019 Sesto Fiorentino, Italy
[3] Department of Industrial and Information Engineering, Second University of Naples, Via Roma 29, 81031 Aversa, Italy

Received 1 December 2015, revised 11 March 2016, accepted 15 March 2016
Published online 19 April 2016

Key words: surface plasmon resonance, plastic optical fibre, C-reactive protein, serum, microfluidic system

A plastic optical fibre biosensor based on surface plasmon resonance for the detection of C-reactive protein (CRP) in serum is proposed. The biosensor was integrated into a home-made thermo-stabilized microfluidic system that allows avoiding any thermal and/or mechanical fluctuation and maintaining the best stable conditions during the measurements. A working range of 0.006–70 mg L^{-1} and a limit of detection of 0.009 mg L^{-1} were achieved. These results are among the best compared to other SPR-based biosensors for CRP detection, especially considering that they were achieved in a real and complex medium, i.e. serum. In addition, since the sensor performances satisfy those requested in physiologically-relevant clinical applications, the whole biosensing platform could well address high sensitive, easy to realize, real-time, label-free, portable and low cost diagnosis of CRP for future lab-on-a-chip applications.

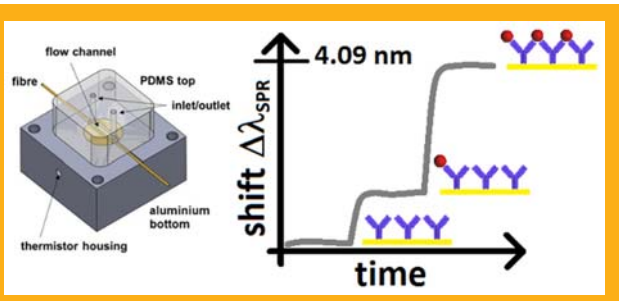

3D sketch (left) of the thermo-stabilized home-made flow cell developed to house the SPR-based plastic optical fibre biosensor. Exemplary response curve (shift of the SPR wavelength versus time) of the proposed biosensor (right) for the detection of C-reactive protein in serum.

1. Introduction

As a pattern recognition molecule, C-reactive protein (CRP) binds to the specific molecular configurations that are typically exposed during cell death or found on the surfaces of pathogens [1]. Its level in real samples is routinely determined for many clinical purposes, being this analyte related to many different pathologies: for example, its measurement can be of great help to identify the reasons of inflammation in lymph nodes, which can be associated to cancer or the causes of deficiency of the immune system. Moreover, it can provide a substantial link between inflammation, fibrosis and atherosclerosis [2], as well as important information on obstructive sleep apnoea by monitoring in parallel the level of inter-

* Corresponding author: e-mail: c.trono@ifac.cnr.it, Phone: +39 055 522 6359, Fax: +39 055 522 6400
** These authors contributed equally to this work.

leukin-6 (IL-6) [3]. Therefore, high levels in serum are observed after trauma, tissue necrosis, infection, surgery, and myocardial infarction and are associated with an increased risk of cardiovascular diseases, especially coronary heart disease risk, which is a leading cause of death in adults. In the case of these kinds of infection and acute inflammatory events, the CRP concentration may increase up to 1000-fold [4]. It is worth mentioning that the concentration of CRP in healthy human serum is lower than 1 mg L^{-1} (low risk), slightly increasing with aging, and it increases beyond 3 mg L^{-1} in case of high risk [5, 6].

The optical platforms available on the market able to detect CRP are essentially based on enzyme-linked immunosorbent assay (ELISA) [7–9], which is a well-established method with a limit of detection (LOD) down to 0.2 mg L^{-1} (high sensitive CRP-ELISA) [8]. However, because of non-specific binding, this procedure has the disadvantage of a relatively high false positive rate caused by different phenomena, such as non-specific immunoglobulin deposition on the ELISA plate plastic material [10–12]. The other problem is the influence of the medium composition and colour on the response, which in turn limits the implementation of this technique in clinical analysis of some diseases such as inflammatory bowel disease (IBD), like Crohn's disease and ulcerative colitis [13] and colon cancer [14].

To overcome these problems and also to provide more accurate tools for earlier diagnosis, in recent decades, additional strategies for CRP detection have been proposed. A CRP assay by using a magnetic permeability detector with LOD of 0.2 mg L^{-1} [15] or magnetic nanoparticles conjugated with anti-CRP antibody with LOD of 0.12 mg L^{-1} [16], the use of the chemiluminescence signal related to CRP-specific DNA aptamer integrated in a microfluidic system with LOD of 0.0125 mg L^{-1} [17], a laser nephelometry method with LOD down to 0.04 mg L^{-1} [18] and a novel fluorescence-based optical platform [19] are some of the techniques that have been developed during the past few years.

Alternatively, the development of surface plasmon resonance (SPR)-based biosensor platforms with the ability to monitor the sample binding process in real-time without labelling, thus providing an application oriented to a specific target molecule, represents a consolidated and high performance solution [20, 21]. With this technique, surface plasmon polaritons (SPPs) are exploited which are generally achieved via the attenuated total reflection method based on a prism or waveguide couplers. These transverse electromagnetic waves propagate along the metal-dielectric boundary and are highly sensitive to the local change in the refractive index (RI) of the surrounding medium, which in turn depends on the interaction between a bio-molecular recognition element (i.e. antibody, protein, DNA, bacteria, etc.), immobilized on the surface of metal, and the desired analyte [22]. The resulting RI change and, accordingly, the variation of SPR condition depend on the concentration of target analyte. High sensitivity and resolution, low LOD, versatility, real-time response, direct and label-free detection of target species, continuous monitoring as well as complete analyses are provided by means of SPR-based biosensors [20–22].

Different configurations of SPR-based biosensors for various bio-applications have been proposed in literature, with the sensing layer deposited on suitable metallic substrates, realized, for example, on planar chips or optical fibres [23–25]. One of the first example of a complete SPR-based biosensor for the CRP detection using two different anti-CRP antibodies (clone C2 and C6, monoclonal, IgG) was characterized by a LOD of 2 mg L^{-1} and a linear detection range of 2–5 mg L^{-1} [5]. The value of LOD of a similar SPR-based bioassay for CRP detection was further reduced to 1 mg L^{-1} [26]. By using a highly sensitive molecular recognition layer of E. coli outer membrane with Z-domains (larger number of analyte binding sites at the same unit area) deposited on a SPR biosensor, LOD for CRP was greatly improved down to 0.0015 mg L^{-1} [27].

The aim of this study is the development of an SPR-based fibre sensor with antibody-antigen assay to detect CRP. The sensing platform presented here uses a side-polished multimode plastic optical fibre (POF) as the light guiding structure, which has particular advantages due to its low cost, easy manipulation, excellent flexibility, great numerical aperture and large diameter, along with the fact that plastic is able to withstand smaller bend radii than glass [28]. Gold is chosen as the plasmonic responsible layer in the sensor platform because of the extremely well understood chemical interaction with organic compounds and its good resistance to oxidation and corrosion in different environments [29]. In addition, the gold-coated in-POF sensor is integrated into a new thermo-stabilized microfluidic platform.

The results which will be presented demonstrate that a very good limit of detection for CRP, even in serum, can be reached with this sensing platform with advantages respect to other traditional SPR systems in terms of cost, easy-to-use and dimensions.

2. Experimental

2.1 Materials

Ethanol (EtOH), 11-mercaptoundecanoic acid, bovine serum albumin (BSA) and all the reagents for

buffer preparation (phosphate-buffered saline (PBS), 40 mM, pH 7.4) were purchased from Sigma-Aldrich (Milan, Italy). C-reactive protein (CRP) (purified antigen) was purchased from Biodesign (Saco, USA). The mouse monoclonal antibody anti-CRP, clone C5, was from Meridian Life Science (Memphis, USA). 1-Ethyl-3-[3-dimethylaminopropyl] carbodiimide hydrochloride (EDC) and N-hydroxysuccinimide (NHS) were purchased from Pierce (Illinois, USA). Human serum (C Reactive Protein Free Serum) was purchased by HyTest Ltd. (Turku, Finland). Polydimethylsiloxane (PDMS) (Sylgard® 184 silicone elastomer kit) was purchased from Dow Corning (Wiesbaden, Germany).

2.2 Optical setup and microfluidic system

The optical sensor was realized as described in Ref. [28]. Briefly, 1 mm plastic optical fibre (PMMA core of 980 μm and a fluorinated polymer cladding of 20 μm) was polished for a length of 10 mm and for a depth of roughly 150 μm, removed along half the circumference and the exposed core was then covered by spin coating with a buffer photoresist (Microposit S1813). The 10 mm-long sensing region was finally realized by sputtering a thin gold film by using a sputtering machine (Bal-Tec SCD 500).

The optical setup employed to measure the light spectrum transmitted through the SPR sensor was composed of a halogen lamp, illuminating the sensor system, and a fibre optic spectrometer. The employed halogen lamp (Carl Zeiss CLH 500) exhibits a wavelength emission range from 380 nm to 1140 nm, whereas the employed spectrometer (Ocean Optics S2000) provides a detection range from 230 nm to 910 nm. The SPR transmission spectrum of each solution was obtained by measuring the transmission spectrum normalized to the spectrum achieved in air as surrounding medium (reference spectrum). The resonance peak in the transmission spectrum corresponds to the excitation of the SPR signature. The value of the SPR wavelength (λ_{SPR}) was achieved by fitting the resonance peak by means of the Gaussian function using OriginPro 8.5 software tool.

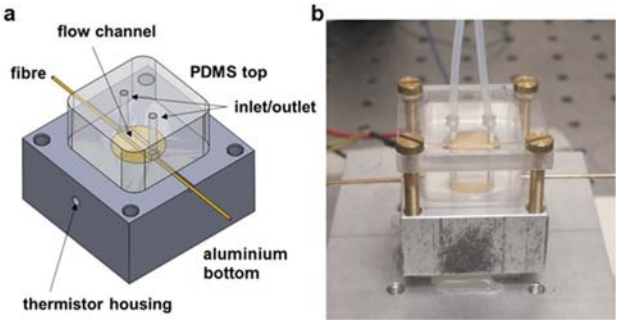

Figure 1 The 3D sketch (**a**) and the picture (**b**) of the thermo-stabilized home-made flow cell developed for housing the SPR-based biosensor. The microfluidic system consists of two parts, PDMS top part and aluminium bottom one. A Peltier element for the temperature stabilization of the system is placed between the aluminium part and a heat-sink.

For the measurements, the sensor was housed inside a home-made flow cell illustrated in Figure 1. The 3D sketch of the cell consists of an aluminium bottom and a PDMS top part (Figure 1a). The aluminium bottom part (30 mm × 30 mm × 15 mm) contains the housing for the sensor head, the groove housing for the POF and the housing for a thermistor. The PDMS top part (20 mm × 20 mm × 10 mm) contains the flow channel (9.5 mm × 2 mm × 1 mm, volume 20 μL) and the inlet and outlet.

The sensor fits perfectly into the sensor frame housing manufactured into the aluminium bottom part and thermal grease was used in order to optimize the thermal conduction. When the PDMS part is placed on the top, the flow channel fits only in the area where there is the sensing region of the optical fibre. The PDMS top part can be pressed onto the bottom part and on the cylindrical plastic frame of the sensor by means of a PMMA slide and four screws, as shown in the picture of Figure 1b. The aluminium bottom part of the flow cell is placed in thermal contact with a Peltier cell (20 mm × 20 mm), located over the heat-sink (see Figure 1b). A Thermo-Electric-Cooling (TEC) driver (ILX LIGHTWAVE LDC-3722B) acquires the temperature from the thermistor inserted into the lateral hole of the aluminium part and drives the current to the Peltier cell in order to stabilise the temperature in the flow channel during the measurement.

2.3 Assay protocol

A solution of 11-mercaptoundecanoic acid 0.5 mM in a H_2O/ethanol solution (10% ethanol) was used to functionalize the gold surface of the sensor. The thiol solution was left in contact with the gold layer for 12 hours. The functionalized sensor was then housed inside the temperature-stabilized flow cell. All the steps for the implementation of the immunoassay were performed using the flow cell connected to a peristaltic pump and keeping the temperature of the flow cell at (23 ± 0.1) °C. The preparation of the CRP-selective bio-layer consisted of the following steps: activation of –COOH groups by cross-linking chemistry (200 mM EDC and 50 mM NHS) for 15 minutes, covalent immobilization of anti-CRP antibody (1 g L^{-1} in PBS) for 40 minutes, washing with PBS for 5 minutes to remove the un-

reacted antibodies, and surface passivation with BSA (1% in PBS) for 15 minutes in order to block the remaining activated carboxylic groups and to prevent non-specific adsorption onto the surface.

The antigen binding steps, with increasing concentrations of CRP ranging from 10 μg L^{-1} up to 500 mg L^{-1} in human serum (diluted 1 : 10 (v/v) in PBS), were performed by flowing the antigen solution inside the flow channel for 15 minutes followed by a washing step with PBS for 5 minutes.

Each step of the assay protocol was monitored in real-time with the previous described experimental setup and a spectrum was collected every 2 minutes during the bio-layer preparation and every 1 minute during the binding interactions.

3. Results and discussion

In order to evaluate the excitation of the SPR signature, the spectrum was recorded by considering the sensor in two different situations: before and after its housing into the developed flow cell.

Figure 2 shows the spectra of the sensor placed outside (in blue) and inside (in red) the manufactured microfluidic system, when a drop of de-ionized water (RI = 1.333 RIU, refractive index unit) was deposited on the sensor surface through manual pipetting (sensor outside) or a solution of PBS (RI = 1.334 RIU) was injected into the flow cell (sensor inside). Only one resonance peak at 667.1 nm was clearly distinguishable from noise when the sensor was outside its

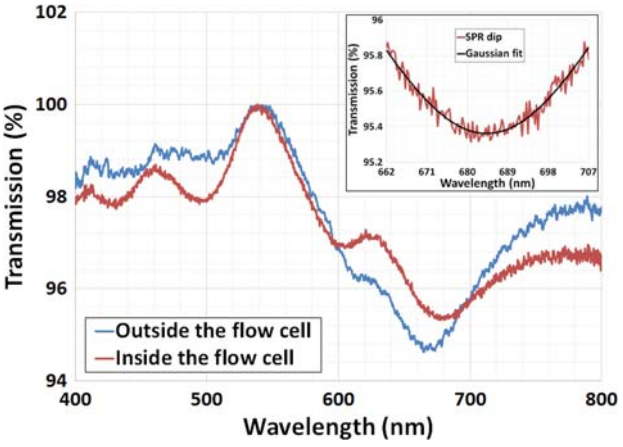

Figure 2 Sensor spectra outside (in blue) and inside (in red) the flow cell normalized to the sensor spectrum in air taken as reference. By comparing these two spectra, the resonance peak corresponding to the excitation of the SPR signature is the only one at longer wavelengths, such as at 667.1 nm (sensor outside) or at 684.6 nm (sensor inside). The inset shows the enlargement of the SPR resonance peak at 684.6 nm along with its fitting (in black) by means of the Gaussian function.

housing. Conversely, four resonance peaks at 431.5 nm, 494.6 nm, 605 nm and 684.6 nm were clearly observed in the transmission spectrum when the sensor was inside the flow cell. It is worth pointing out that, in optical fibre sensors based on SPR, the spectrum is the result of the convolution of different resonance peaks. Each peak is obtained for a specific resonance condition defined by a given angle-wavelength pair [30]. However, by comparing these two spectra, the resonance peak corresponding to the excitation of the SPR signature is the only one at longer wavelengths, which also experienced a red-shift (i.e. shift at longer wavelengths). Therefore, for the rest of the work, the fourth resonance peak at 684.6 nm will be taken into account. The measured red-shift of 17.5 nm of the SPR signature can be ascribed to the contribution of two effects: considering the bulk RI sensitivity of the sensor approaching 10^4 nm RIU^{-1} [30], the first (and primary) effect is related to the difference between the RI of PBS and water ($\Delta RI = 10^{-3}$ RIU), whereas the second (and secondary) one is due to the mechanical stress induced on the sensor once it is housed into the flow cell. Moreover, the inset of Figure 2 details the enlargement of the SPR resonance peak along with its fitting (in black) by means of the Gaussian function as an example of the procedure used to extrapolate the value of λ_{SPR} and mentioned in the previous section.

In addition, as shown in Figure 2, the signal-to-noise ratio (SNR) remains almost comparable when the sensor is placed inside the flow cell even with a reduction of both mechanical and temperature fluctuations. On the other hand, this last issue is crucial in the case of biochemical sensing when very low RI changes should be reliably measured [31]. Reduced fluctuations and thermal stabilization decrease the standard deviation of measurement and thus improve the sensor resolution.

After the functionalization of the surface of the gold-coated side-polished POF with the thiol solution, all the steps of the assay protocol described in the previous section were recorded in real-time. First, the effect of the immobilization of the capture antibody (anti-CRP 1000 mg L^{-1}) was carefully investigated. Figure 3 shows the binding interaction of the anti-CRP immobilization and the subsequent washing with PBS. Two different steps are detailed: the anti-CRP immobilization by filling the flow cell with anti-CRP for 40 minutes at a flow rate of 10 μL min^{-1} and then the washing with PBS for 5 minutes at a flow rate of 150 μL min^{-1}. The first step is characterized by an increase in the λ_{SPR}, with a shift of $\Delta\lambda_{SPR} = 1.53$ nm. The figure accounts also for the fitting of the experimental data (solid grey line) by means of the exponential function ($A \cdot e^{-t/\tau}$). The time to reach the saturation, the condition of which all the free surface functionalities are occupied, was found to be about 35 minutes.

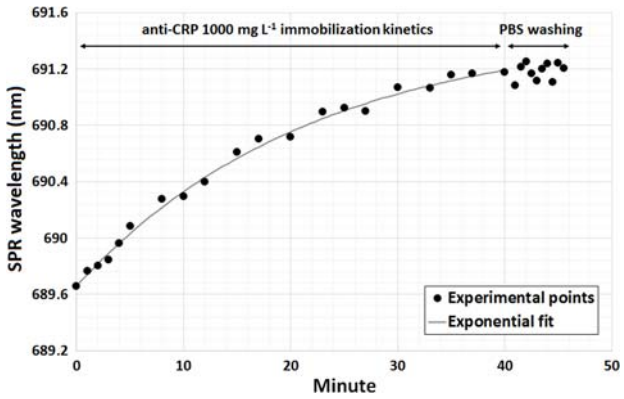

Figure 3 Binding interaction of immobilization of the capture antibody (1000 mg L^{-1} anti-CRP) for 40 minutes at a flow rate of 10 µL min^{-1} and the subsequent washing in PBS buffer for 5 minutes at a flow rate of 150 µL min^{-1}. The total shift of the SPR wavelength is 1.53 nm. The fitting of the experimental data (solid grey line) related to the anti-CRP immobilization by means of the exponential function is also detailed.

It is worth highlighting that the value of λ_{SPR} at the end of the capture immobilization process remained unchanged also during the subsequent washing with PBS. The reason could rely on the full coverage along the sensor surface by the capture antibodies, meaning that the capture antibodies were covalently attached on the sensor surface. The increase of noise during the washing could be due to the flow rate, which was 5 times higher than that during the binding interaction. This higher flow rate probably caused some small temperature fluctuations.

As an example, one antigen concentration (1 mg L^{-1} CRP) was taken into account with the aim of showing the CRP binding interaction. As in the previous figure, two different steps are detailed in Figure 4: the binding interaction by filling the flow cell with CRP solution for 15 minutes at a flow rate of 30 µL min^{-1} and then the washing with PBS for 5 minutes at a flow rate of 150 µL min^{-1}. During the binding of this CRP concentration, the SPR wavelength λ_{SPR} exhibited a shift of $\Delta\lambda_{SPR} \approx 0.8$ nm. By fitting the experimental data (solid grey line) with the single exponential function, the time to reach the plateau was roughly 10 minutes, providing an estimation of the binding time. This curve shows the typical exponential behaviour with a saturation, proving that the antibody/antigen interaction reached the equilibrium condition [32]. This also occurred for all the antigen (CRP) concentrations (data not shown). Even in this case, an increase of the noise during the washing step was observed.

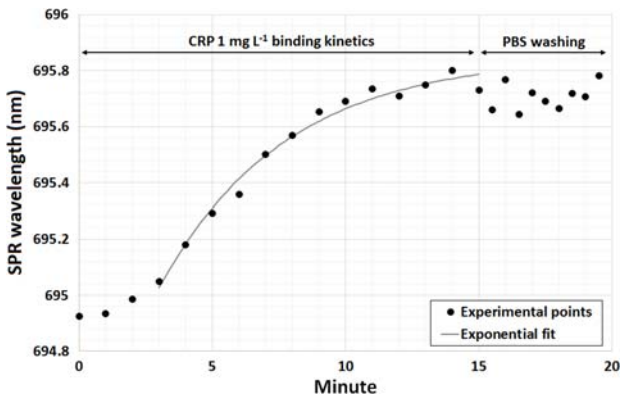

Figure 4 Example of the binding interaction of the specific antigen (1 mg L^{-1} CRP) for 15 minutes at a flow rate of 30 µL min^{-1} and the subsequent washing in PBS buffer for 5 minutes at a flow rate of 150 µL min^{-1}. The total shift of the SPR wavelength is 0.8 nm. The fitting of the experimental data (solid grey line) related to the CRP binding by means of the exponential function is also shown.

In order to measure the real shift of SPR wavelength just related to the CRP binding, a washing step in buffer is necessary after each CRP binding interaction. In fact, the important measurand is represented by the surface RI changes induced by the interactions between the immobilized captures (anti-CRPs) and the specific analytes (CRPs) along the functionalized surface, and not by the bulk RI changes related to the refractive index of the solution pumped inside the flow cell [31, 32].

The wavelength of the SPR signature λ_{SPR} as a function of the CRP concentration is shown in Figure 5, along with the fitting (correlation factor of 0.993) through the logistic curve that is a well-accepted mathematical model for describing the sigmoidal response of a biosensor [33]. The value of each experimental point is given by the average of

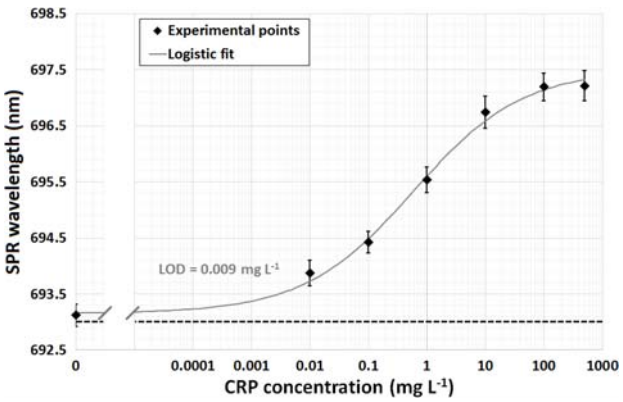

Figure 5 Calibration curve of the developed CRP biosensor in serum showing the SPR wavelength as a function of the analyte concentration. Each experimental point (black rhombuses) is the average of 15 subsequent measurements and the respective standard deviations (black error bars) are also shown. The solid grey line provides the best sigmoidal curve fitting to the experimental data. The dashed black line indicates the value of λ_{SPR} PBS before the addition of serum not spiked with CRP.

15 values measured stopping the flow after each PBS washing step, thus preventing any fluctuation and maintaining the best stable measuring conditions. The corresponding standard deviation of each experimental point is also detailed in Figure 5 as black error bars. The experimental point at 0 mg L^{-1} of CRP concentration is the measured value of the λ_{SPR} taken in serum before the exposure to any CRP concentration.

From the calibration curve of Figure 5, it is possible to extrapolate some parameters, such as the dynamic signal range (DSR), the working range (WR) and the limit of detection (LOD) of the biosensor. The DSR is the difference between the two horizontal asymptotes of the sigmoidal curve, $\lambda_{SPR,max}$ and $\lambda_{SPR,min}$. The WR is calculated by considering the antigen concentration range between 10% and 90% of the dynamic signal range [34], whereas the LOD is evaluated as three times of the standard deviation of the blank measurement, which is the measurement achieved with serum, following the IUPAC recommendation [35]. From the calibration curve of Figure 5, the value of the asymptotes are $\lambda_{SPR,max}$ = 697.5 nm and $\lambda_{SPR,min}$ = 693.2 nm. Accordingly, the values of DSR and WR are 4.3 nm and 0.006–70 mg L^{-1}, respectively. Finally, the LOD for the proposed biosensor can be estimated as 0.009 mg L^{-1} ($3\sigma = 0.59$ nm).

A very good specificity was also demonstrated by the sensor as evidenced in Figure 5, where the signal obtained in PBS before the addition of serum not spiked with CRP (dashed black line in Figure 5) has been included in the plot for comparison with the serum signal (first point in the calibration). Negligible difference, within the standard deviation, among the PBS and serum signals can be observed from the figure. Human serum is in this case a very good control, since this serum is declared to be CRP-free, but it contains all the other proteins naturally present in serum, among which human serum albumin, immunoglobulins and transferrin represent more than the 70% of the total protein serum content [36].

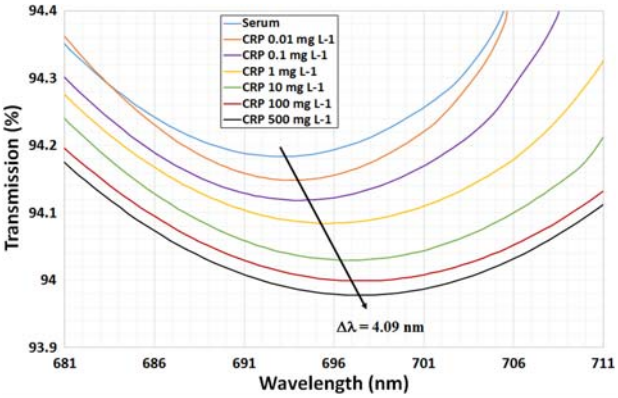

Figure 6 Fitted spectra of the SPR resonance peak during the development of the immunoassay, starting from the flowing of serum and up to the increasing concentrations of CRP (as detailed in the figure legend). The total red-shift of the λ_{SPR} is roughly 4.1 nm.

As an example, Figure 6 accounts for the fitted spectra of the considered SPR resonance peak and its evolution during the development of the immunoassay, starting from the flowing of serum and up to the increasing concentrations of CRP (as detailed in the figure legend). The total red-shift of the λ_{SPR} is roughly 4.1 nm in compliance with the value of DSR.

The performance of the proposed biosensor was compared with other SPR-based biosensors for the detection of CRP in terms of the sensor configuration, the matrix type and the claimed sensor performance. Most of the papers only provide the sensitiv-

Table 1 Comparison of the performances of SPR-based biosensors for the detection of CRP.

Sensing method	Matrix type	LOD	Ref.
Fluorescence	Human plasma	30 µg L^{-1}	[37]
Fluorescence	Serum	20 µg L^{-1}	[38]
ELISA	PBS and serum	1 µg L^{-1}	[39]
Chemi-luminescence (magnetic beads)	Serum	12 µg L^{-1}	[40]
SPR	Tris + calcium	1 mg L^{-1}	[12]
SPR	PBS	2 mg L^{-1}	[5]
SPR	PBS and serum	1.5 µg L^{-1}	[41]
SPR	HEPES at pH 6.5 + calcium	5 µg L^{-1}	[42]
Evanescent field technology	Human serum	[a]55 µg L^{-1} [b]130 µg L^{-1}	[34]
Etched FBG coated with graphene oxide	Serum	10 µg L^{-1}	[43]
Magnetic permeability detector	Human plasma	0.2 mg L^{-1}	[44]
Magnetic nanoparticles under magnetic fields	Serum	0.12 mg L^{-1}	[16]
Quartz crystal microbalance	Serum	0.13 µg L^{-1}	[45]
Impedance spectroscopy	Blood serum	19 µg L^{-1}	[46]

[a] Binding inhibition assay
[b] Sandwich assay

ity (the shift of the selected resonant peak relative to a selective RI range) or the resolution (the minimum measurable RI change distinguishable from the noise), whereas just few papers provide the value of LOD for the investigated analyte. Table 1 summarises some of the most detailed results reported in literature. The results achieved with the proposed sensing system (WR of 0.006–70 mg L^{-1} and LOD of 0.009 mg L^{-1}) are competitive in the field of optical fibre biosensors based on SPR for the detection of CRP, especially considering that they were achieved in a complex matrix such as serum. Very good performances with respect to the other traditional SPR systems can be evidenced if considering that most of the published CRP SPR biosensors [5, 12, 42] have been tested only in buffer solutions without proving the sensor usability in real sample matrices, such as serum, and that the reached LOD of 9 μg L^{-1} is among the best LODs also of biosensors not based on SPR. Moreover, advantages with respect to other traditional SPR systems or other magnetic or electrochemical techniques, are represented by the low cost, easy-to-use, flexibility and portability of the developed SPR plastic optical fibre biosensor.

4. Conclusion

A plastic optical fibre biosensor based on surface plasmon resonance for the detection of C-reactive protein in serum was presented. The biosensor was integrated into an ad-hoc developed thermo-stabilized microfluidic system that allowed to avoid any thermal and/or mechanical fluctuation and to maintain the best stable conditions during the measurements. A dynamic signal range of 4.3 nm, a working range of 0.006–70 mg L^{-1} and a LOD of 0.009 mg L^{-1} were achieved. These results are among the best compared to other SPR-based biosensors for CRP detection, especially considering that they were achieved in a real and complex medium, i.e. serum (see Table 1). Since the sensor performances are those requested for many clinical purposes, the whole biosensing platform could well address the continuous request of the physicians for high sensitive, easy to realize, real-time, label-free, portable and low cost sensing platforms for future lab-on-a-chip applications.

Acknowledgements

The authors wish to thank Dr. Chiara Berrettoni for her assistance in graphic development and improvement. F.C. wishes to thank the Italian Minister of University and Research (MIUR) under the grant N. RBFR122KL1. S.T. wishes to thank the European Community for the project Hemospec (FP7-611682).

Author biographies Please see Supporting Information online.

References

[1] S. Black, I. Kushner, and D. Samols, J. Biol. Chem. **279**, 48487–48490 (2004).
[2] S. P. Mazer and L. E. Rabbani, J. Thromb. Thrombolysis **17**, 95–105 (2004).
[3] J. M. Latina, N. A. M. Estes, and A. C. Garlitski, Pulm. Med. **2013**, 621736 (2013).
[4] R. D. Ramamoorthy, V. Nallasamy, R. Reddy, N. Esther, and Y. Maruthappan, J. Pharm. Bioallied. Sci. **4** (Suppl 2), S422–S426 (2012).
[5] M. H. F. Meyer, M. Hartmann, and M. Keusgen, Biosens. Bioelectron. **21**, 1987–1990 (2006).
[6] B. Clyne and J. S. Olshaker, J. Emerg. Med. **17**, 1019–1025 (1999).
[7] M. D. Parra, M. Tuomola, J. Cabezas-Herrera, and J. J. Ceron, Am. J. Vet. Res. **66**, 62–66 (2005).
[8] R. Dominici, P. Luraschi, and C. Franzini, J. Clin. Lab. Anal. **18**, 280–284 (2004).
[9] J. L. Clarke, J. L. Anderson, J. F. Carlquist, R. F. Roberts, B. D. Horne, T. L. Bair, M. J. Kolek, C. P. Mower, A. M. Crane, W. L. Roberts, and J. B. Muhlestein, Am. J. Cardiol. **95**, 155–158 (2005).
[10] J. Yang, K. W. Joo, Y. S. Kim, C. Ann, J. S. Han, S. Kim, and J. S. Lee, J. Nephrol. **18**, 102–105 (2005).
[11] E. Güven, K. Duus, M. C. Lydolph, C. Sværke Jørgensen, I. Laursen, and G. Houen, J. Immunol. Methods **403**, 26–36 (2014).
[12] W. P. Hu, H. Y. Hsu, A. Chiou, K. Y. Tseng, H. Y. Lin, G. L. Chang, and S. J. Chen, Biosens. Bioelectron. **21**, 1631–1637 (2006).
[13] T. P. Erlinger, E. A. Platz, N. Rifai, and K. J. Helzlsouer, JAMA **291**, 585–590 (2004).
[14] J. C. Cabrera-Abreu, P. Davies, Z. Matek, and M. S. Murphy, Arch. Dis. Child. **89**, 69–71 (2004).
[15] K. Kriz, F. Ibraimi, M. Lu, L. O. Hansson, and D. Kriz, Anal. Chem. **77**, 5920–5924 (2005).
[16] H. Y. Tsai, C. F. Hsu, I. W. Chiu, and C. B. Fuh, Anal. Chem. **79**, 8416–8419 (2007).
[17] W. B. Lee, Y. H. Chen, H. I. Lin, S. C. Shiesh, and G. B. Lee, Sens. Actuators B **157**, 710–721 (2011).
[18] M. Faraj, and N. Salem, in: T. E. Moschandreou (ed.), C-Reactive Protein, Blood cell – An overview of studies in hematology (InTech, 2012), doi:10.5772/47735.
[19] F. Baldini, A. Carloni, A. Giannetti, G. Porro, and C. Trono, Sens. Actuators B **139**, 64–68 (2009).
[20] J. Homola, Chem. Rev. **108**, 462–493 (2008).
[21] M. Piliarik and J. Homola, Opt. Express **17**, 16505–16517 (2009).
[22] C. Caucheteur, T. Guo, and J. Albert, Anal. Bioanal. Chem. **407**, 3883–3897 (2015).

[23] M. Piliarik, H. Šípová, P. Kvasnička, N. Galler, J. R. Krenn, and J. Homola, Opt. Express **20**, 672–680 (2012).
[24] T. Špringer, M. L. Ermini, B. Špačková, J. Jablok, and J. Homola, Anal. Chem. **86**, 10350–10356 (2014).
[25] E. Edy Wijaya, C. Lenaerts, S. Maricot, J. Hastanin, S. Habraken, J. P. Vilcot, R. Boukherroub, and S. Szunerits, Curr. Opin. Solid State Mater. Sci. **15**, 208–224 (2011).
[26] W. P. Hu, H. Y. Hsu, A. Chiou, K. Y. Tseng, H. Y. Lin, G. L. Chang, and S. J. Chen, Biosens. Bioelectron. **21**, 1631–1637 (2006).
[27] J. Jose, M. Park, and J. C. Pyun, Biosens. Bioelectron. **25**, 1225–1228 (2010).
[28] N. Cennamo, D. Massarotti, L. Conte, and L. Zeni, Sensors **11**, 11752–11760 (2011).
[29] N. Cennamo, M. Pesavento, L. Lunelli, L. Vanzetti, C. Pederzolli, L. Zeni, and L. Pasquardini, Talanta **140**, 88–95 (2015).
[30] M. Kanso, S. Cuenot, and G. Louarn, Plasmonics **3**, 49–57 (2008).
[31] F. Baldini, M. Brenci, F. Chiavaioli, A. Giannetti, and C. Trono, Anal. Bioanal. Chem. **402**, 109–116 (2012).
[32] F. Chiavaioli, C. Trono, A. Giannetti, M. Brenci, and F. Baldini, J. Biophotonics **7**, 312–322 (2014).
[33] R. A. Dudley, P. Edwards, R. P. Ekins, D. J. Finney, I. G. McKenzie, G. M. Raab, D. Rodbard, and R. P. Rodgers, Clin. Chem. **31**, 1264–1271 (1985).
[34] C. Albrecht, N. Kaeppel, and G. Gauglitz, Anal. Bioanal. Chem. **391**, 1845–1852 (2008).
[35] J. Inczedy, T. Lengyel, and A. M. Ure, Compendium of analytical nomenclature - The orange book (Blackwell, Oxford, 1998).
[36] D. Docter, U. Distler, W. Storck, J. Kuharev, D. Wünsch, A. Hahlbrock, S. K. Knauer, S. Tenzer, and R. H. Stauber, Nature Protocols **9**, 2030–2044 (2014).
[37] M. Wolf, D. Juncker, B. Michel, P. Hunziker, and E. Delamarche, Biosens. Bioelectron. **19**, 1193–1202 (2004).
[38] V. Raj, P. Hari, M. Antony, and K. Sreenivasan, Sens. Actuators B **146**, 23–27 (2010).
[39] N. Christodoulides, M. Tran, P. N. Floriano, M. Rodriguez, A. Goodey, M. Ali, D. Neikirk, and J. T. McDevitt, Anal. Chem. **74**, 3030–3036 (2002).
[40] Y. N. Yang, H. I. Lin, J. H. Wang, S. C. Shiesh, and G. B. Lee, Biosens. Bioelectron. **24**, 3091–3096 (2009).
[41] I. Vikholm-Lundin, and W. M. Albers, Biosens. Bioelectron. **21**, 1141–1148 (2006).
[42] A. Bini, S. Centi, S. Tombelli, M. Minunni, and M. Mascini, Anal. Bioanal. Chem. **390**, 1077–1086 (2008).
[43] S. Sridevi, K. S. Vasu, S. Asokan, and A. K. Sood, Biosens. Bioelectron. **65**, 251–256 (2015).
[44] H. C. Kim, S. K. Lee, W. B. Jeon, H. K. Lyu, S. W. Lee, and S. W. Jeong, Ultramicroscopy **108**, 1379–1383 (2008).
[45] N. Kim, D. K. Kim, and Y. J. Cho, Sens. Actuators B **143**, 444–448 (2009).
[46] T. Bryan, X. Luo, P. R. Bueno, and J. J. Davis, Biosens. Bioelectron. **39**, 94–98 (2013).